LETTER

https://doi.org/10.1038/s41586-018-0072-8

Earliest known hominin activity in the Philippines by 709 thousand years ago

T. Ingicco[1,2,3,4]*, G. D. van den Bergh[5], C. Jago-on[6], J.-J. Bahain[1,2,3,4], M. G. Chacón[1,2,3,4,7,8], N. Amano[9], H. Forestier[1,2,3,4], C. King[6], K. Manalo[10], S. Nomade[11,12,13], A. Pereira[1,2,3,4,11,12,13,14,15], M. C. Reyes[6,10]*, A.-M. Sémah[1,2,3,4,16], Q. Shao[17], P. Voinchet[1,2,3,4], C. Falguères[1,2,3,4], P. C. H. Albers[18], M. Lising[6,19], G. Lyras[20], D. Yurnaldi[21], P. Rochette[22,23,24,25,26], A. Bautista[6] & J. de Vos[18]

Over 60 years ago, stone tools and remains of megafauna were discovered on the Southeast Asian islands of Flores, Sulawesi and Luzon, and a Middle Pleistocene colonization by *Homo erectus* was initially proposed to have occurred on these islands[1–4]. However, until the discovery of *Homo floresiensis* in 2003, claims of the presence of archaic hominins on Wallacean islands were hypothetical owing to the absence of in situ fossils and/or stone artefacts that were excavated from well-documented stratigraphic contexts, or because secure numerical dating methods of these sites were lacking. As a consequence, these claims were generally treated with scepticism[5]. Here we describe the results of recent excavations at Kalinga in the Cagayan Valley of northern Luzon in the Philippines that have yielded 57 stone tools associated with an almost-complete disarticulated skeleton of *Rhinoceros philippinensis*, which shows clear signs of butchery, together with other fossil fauna remains attributed to stegodon, Philippine brown deer, freshwater turtle and monitor lizard. All finds originate from a clay-rich bone bed that was dated to between 777 and 631 thousand years ago using electron-spin resonance methods that were applied to tooth enamel and fluvial quartz. This evidence pushes back the proven period of colonization[6] of the Philippines by hundreds of thousands of years, and furthermore suggests that early overseas dispersal in Island South East Asia by premodern hominins took place several times during the Early and Middle Pleistocene stages[1–4]. The Philippines therefore may have had a central role in southward movements into Wallacea, not only of Pleistocene megafauna[7], but also of archaic hominins.

The most recent recoveries in Flores[8,9] and Sulawesi[10] (Indonesia) provide a unique documentation of overseas hominin dispersal during the early Middle Pleistocene epoch. An early presence in the Philippine archipelago has been hypothesized since the 1950s, with the reporting of presumably Pleistocene megafaunal remains and 'Palaeolithic' industries consisting of chopping tools and flakes (the 'Cabalwanian' and 'Liwanian' industries, respectively) from surface finds and excavations in the Cagayan Valley basin of northern Luzon[3,4]. Despite the fact that these early discoveries took place more than 60 years ago, no direct association between megafauna and lithic industries has been documented since then, and no secure numerical dating of both fossil fauna and lithics has been available for this region[11]. To date, the discovery of a human metatarsal in Callao Cave in northern Luzon[6], directly dated to 66.7 ± 1.0 thousand years ago (ka), represented the oldest evidence of the peopling of the Philippines.

In 2013, a survey of the Cagayan Valley near the Rizal Municipality (Kalinga Province) led to the discovery of a concentration of vertebrate bones and stone artefacts scattered on the surface near what became our new excavation site. The Kalinga site (17° 33′ 45.0318″ N, 121° 33′ 35.7372″ E) (Fig. 1b) has been excavated annually since 2014 and has resulted in the discovery of in situ megafauna and associated stone artefacts. The substrate consists of the upper part of the Awidon Mesa Formation, a 400-m thick sequence of alluvial stream deposits (mainly sandstones and claystones) intercalated with volcaniclastic and pyroclastic layers (Fig. 1a). These sediments were deposited on an alluvial fan system in braided streams of the paleo-Chico River as a consequence of uplift in the Central Cordillera to the west[12,13]. During a poorly constrained Pleistocene phase of folding in response to east–west compression, alluvial fan deposition in the Kalinga area came to a halt.

We conducted the main 16-m^2 excavation at the head of a modern, dry stream valley, north of a small hill and down to a maximum depth of 2 m (Fig. 1c and Supplementary Information). A 25×1-m^2 slot trench was excavated down the hill to the main excavation. Together, these excavations revealed a total of 7.5 m of stratigraphy comprising four main sedimentary units, in ascending order: unit A, unit F, unit G and unit J (Fig. 1d, e and Extended Data Fig. 1). An almost-complete disarticulated skeleton of *R. philippinensis* (Extended Data Fig. 2) was found embedded in the basal sediments of unit F lying across the base of an erosional channel surface that cuts down vertically into sandy unit A. This channel was filled with an up to 3.25-m thick mudflow (unit F; see Extended Data Fig. 3, 4), which covered the bones, along with an in situ tektite as well as 57 stone tools and sparse fossils of other animals (Geoemydidae, *Varanus* cf. *salvator*, *Stegodon* cf. *luzonensis* and *Cervus* cf. *mariannus*) (see Supplementary Information). The archaeological layer (unit F) is conformably overlaid by an approximately 1.15-m thick, sterile, cross-bedded coarse sandy fluvial unit with silty lenses (unit G), which is in turn conformably overlaid by unit H, a 2.5-m thick silty pedogenized layer with rhyzoliths.

The 57 stone artefacts account for six cores, 49 flakes and two possible hammer stones that all originated from unit F (Fig. 2 and Supplementary Information). With the exception of the two possible hammer stones (Fig. 2b), all artefacts lack a patinated lustre and have a fresh appearance, indicating that any transport was minimal. The knapping strategies were oriented towards short and unorganized core reduction, resulting in non-standardized flake morphologies and dimensions, and all artefacts lacked any intentional retouch.

[1]UMR 7194, CNRS, Paris, France. [2]Département Homme et Environnement, Muséum national d'Histoire naturelle, Paris, France. [3]Université de Perpignan Via Domitia, Perpignan, France. [4]Sorbonne Université, Paris, France. [5]Centre for Archaeological Science, School of Earth and Environmental Sciences, University of Wollongong, Wollongong, New South Wales, Australia. [6]National Museum of the Philippines, Manila, Philippines. [7]IPHES – Institut Català de Paleoecologia Humana i Evolució Social, Tarragona, Spain. [8]Area de Prehistoria, Universitat Rovira i Virgili (URV), Tarragona, Spain. [9]Max Planck Institute for the Science of Human History, Jena, Germany. [10]Archaeological Studies Program, University of the Philippines Diliman, Quezon City, Philippines. [11]Laboratoire des Sciences du Climat et de l'Environnement, CEA, Gif Sur Yvette Cedex, France. [12]UMR 8212, CNRS, Gif Sur Yvette Cedex, France. [13]Université Paris-Saclay, Gif Sur Yvette Cedex, France. [14]Ecole française de Rome, Roma, Italy. [15]Sezione di scienze preistoriche e antropologiche, Dipartimento di Studi Umanistici, Università degli Studi di Ferrara, Ferrara, Italy. [16]Institut de Recherche pour le Développement, UMR LOCEAN 7159, Bondy, France. [17]School of Geographical Sciences, Nanjing Normal University, Nanjing, China. [18]Naturalis Biodiversity Center, Leiden, Netherlands. [19]Department of Sociology and Anthropology, Ateneo de Manila University, Quezon City, Philippines. [20]Faculty of Geology and Geoenvironment National and Kapodistrian University of Athens, Athens, Greece. [21]Centre for Geological Survey, Geological Agency, Bandung, Indonesia. [22]Aix-Marseille Université, Aix en Provence, France. [23]UM34 CNRS, Aix en Provence, France. [24]IRD, Aix en Provence, France. [25]Collège de France, Paris, France. [26]CEREGE, Aix en Provence, France. *e-mail: ingicco@mnhn.fr; mariancreyes@gmail.com

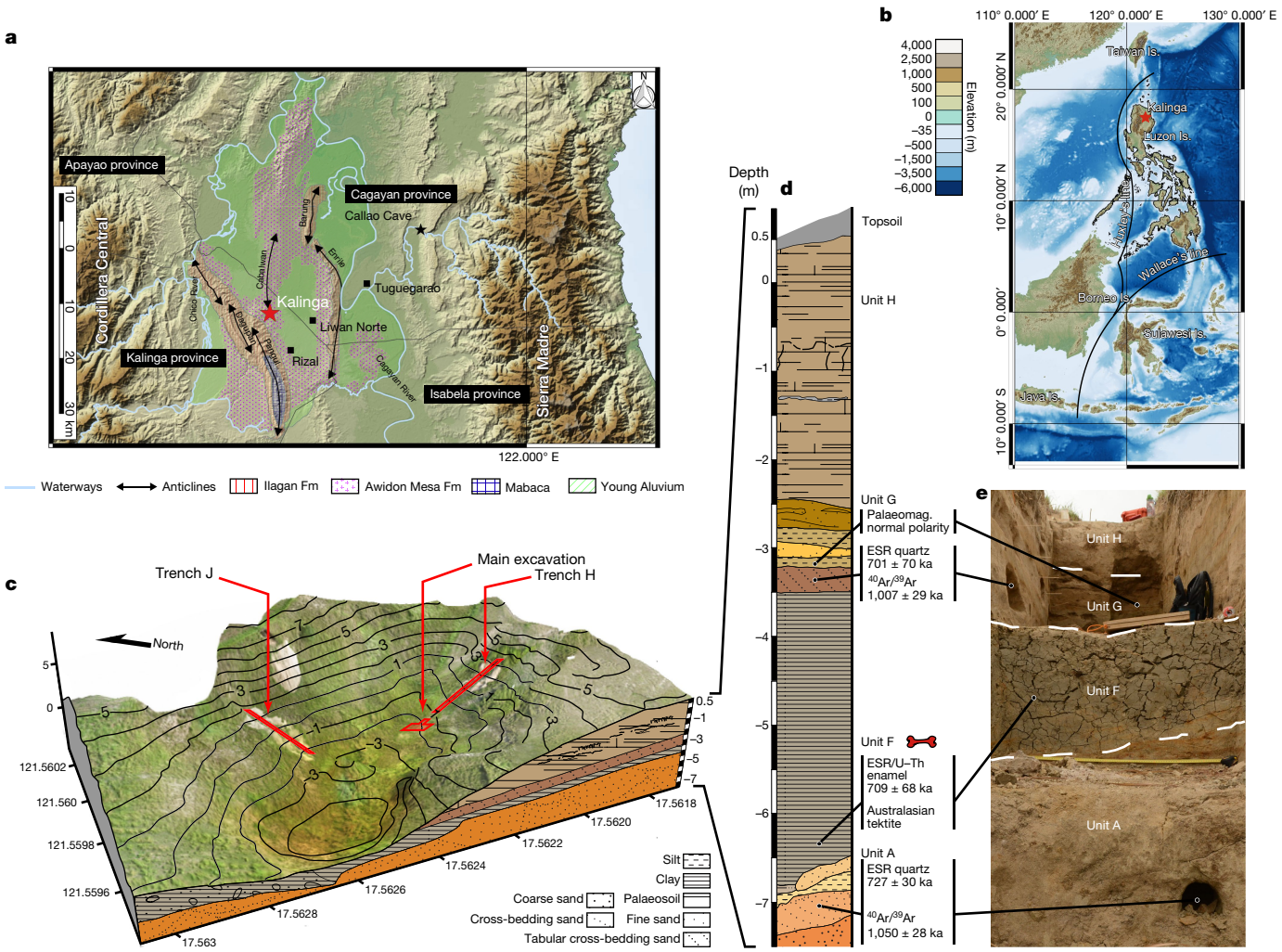

Fig. 1 | Geology and sedimentology of the Kalinga Excavation site. **a**, Digital elevation map of the Cagayan Valley surrounding the Rizal municipality (located in **b**, Northern Luzon Island, east of Huxley's and north of the Wallace Lines). The Kalinga site (red star) is located at the southern tip of the weakly folded Cabalwan Anticline. Geological units of the area bounded by the Cagayan River on the east and the Chico River on the west are after Mathisen[13]. Stratigraphically, the site layers pertain to the upper part of the Awidon Mesa Formation, a Pleistocene sequence of alluvial stream deposits intercalated with volcaniclastic and pyroclastic deposits. The depositional environment of the Awidon Mesa Formation was characterized by braided rivers on an alluvial fan system that formed in response to uplift in the Cordillera Central to the West[12,13]. **c**, Contour map of the main excavation and the adjoining trench H along the small valley where the Kalinga site is located. **d**, Detailed stratigraphy of the excavation with the absolute ages of the sedimentary units. Unit A constitutes a fining upward complex of sandy to silty cross-bedded fluvial sediments. The top of unit A is eroded and cuts down vertically over at least 2.5 m. This erosive channel is filled with unit F, a poorly sorted mudflow deposit with a maximum thickness of 3.25 m. The rhinoceros skeletal elements and most of the stone artefacts were found lying directly above the erosional contact, and were found embedded in the clay-rich mud of unit F. Unit F is conformably overlaid by a sequence of horizontally layered coarse sandy to silty layers (unit G), which is in turn conformably overlaid by a thick sequence of silty deposits overprinted by palaeosols (unit H). **e**, Southward view of trench H showing the lower and upper contacts between mudflow unit F and sandy unit G and between sandy unit A and mudflow unit F.

The Kalinga lithic assemblage is diverse in its techniques, technology and final products, and appears similar to the chert industry described at the Arubo 1 site[14] (see Supplementary Information). Also recovered from the unit F excavation area was a 600-g pebble among hundreds of pebbles that were all lighter than 200 g, and which we interpret as a possible manuport.

Among the more than 400 bones recovered from unit F, the most striking remains were of a disarticulated, approximately 75% complete skeleton of a single *R. philippinensis* individual (Fig. 3 and Extended Data Fig. 2). The bones were found lying on top of the erosional surface down-cutting unit A, and were embedded in the basal clay-rich sediments of unit F along the deepest part of the paleo-channel bed (Extended Data Fig. 3). Although none of the rhinoceros bones were found articulated, the recovered skeletal elements occur within a 3 × 2-m^2 area, suggesting that disarticulation occurred sub-aerially and that transport prior or during deposition of mudflow unit F was minimal.

Thirteen of the excavated rhinoceros bones, all of which in life had a thin cover of soft tissue (that is, the ribs and metacarpals)[15,16], display cut marks (Fig. 3 and Extended Data Fig. 2). Both rhinoceros humeri have similar percussion marks on the anterior surface for the right humerus and on the posterior surface for the left humerus, and both were presumably made with the intention to smash the bones and gain access to the marrow[17]. This percussion action resulted in the breakage of the left humerus into five pieces, which is the only bone found fragmented; however, the fragments were still clustered together within a small 1-m^2 area of the excavation. On the right humerus, however, percussion did not result in the fragmentation of the bone (Fig. 3).

To constrain the age of the bone bed and the stone artefacts it contained, we applied three different dating methods to various materials (Fig. 1). Single crystal ^{40}Ar/^{39}Ar dating was applied to plagioclase

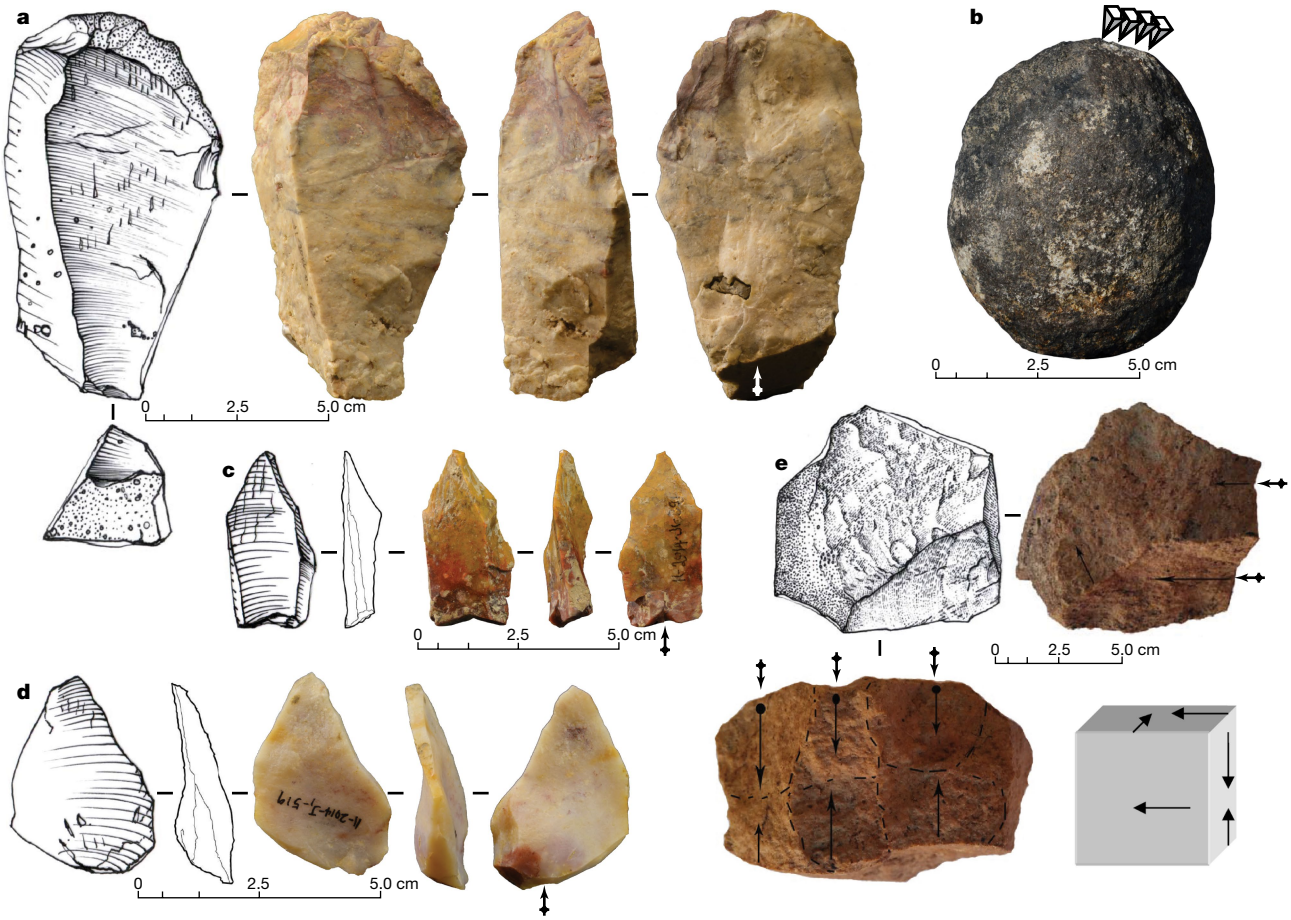

Fig. 2 | Lithic artefacts from Kalinga. a, Cortical flake on chert (II-2014-J1-362; length (L) = 100 mm, breadth (B) = 55 mm, thickness (T) = 33 mm). **b**, Possible hammerstone on dacite (II-2014-J1-371), although its highly eroded aspect precludes any definitive conclusion. Arrows indicate crushed areas interpreted as the result of precussions. **c**, Siret kombewa flake on jasper (II-2014-J1-391; L = 40 mm, B = 18 mm, T = 8 mm) that has a longitudinal and oblique fracture on the inferior two-thirds of the left side resulting from a knapping accident while flaking. **d**, Double-backed flake on flint (II-2014-J1-519). **e**, Core on quartz (II-2014-J1-396), with clear marks of knapping on an anvil, and its diachritic diagram. Arrows indicate the percusion axes.

crystals from the sandy units directly below and above the archaeological unit F and yielded two statistically undistinguishable weighted mean dates of 1,050 ± 28 ka and 1,007 ± 29 ka, respectively (1σ confidence interval; Supplementary Information and Extended Data Fig. 5). These $^{40}Ar/^{39}Ar$ dates yielded an age for the formation of the volcanic plagioclase crystals. Quartz grains from the same two sandy units were also dated using the electron spin resonance (ESR) method[18], and resulted in a maximum depositional date of 727 ± 30 ka for unit A, and a minimum depositional date of 701 ± 70 ka for unit G (1σ confidence interval; see Supplementary Information).

To directly constrain the age of the rhinoceros skeleton and the cut marks, we applied ESR/uranium-series dating to the enamel of the rhinoceros's right maxillary third premolar from the unit F bone bed. The tooth yielded an age of 709 ± 68 thousand years (1σ confidence interval), which is in agreement with the ESR results on the quartz (Fig. 1, Extended Data Fig. 6, Extended Data Table 1, Supplementary Information and Supplementary Table 1). In addition, a palaeomagnetic sample was taken from a laminated silty lens in the lower part of unit G and was found to have a normal magnetic polarity (see Supplementary Information: and Extended Data Fig. 7). The presence in unit F of a reworked Australasian tektite (see Supplementary Information and Extended Data Fig. 8) that had formed during a major meteoritic impact just before the onset of the Brunhes Normal polarity epoch at 781 ka[19,20], also provides further support for these closely grouped dating results. These results further suggest that the volcanic plagioclase crystals from unit G on which the $^{40}Ar/^{39}Ar$ date was obtained were reworked from older volcanoclastic deposits, and therefore provide a maximum age for the sequence (see Supplementary Information). Taken together with the ESR dating results, it follows that the rhinoceros skeleton was buried by a mudflow at least 631 ka.

Our excavations at Kalinga and the numeric dating results clearly provide securely dated evidence for human colonization of the Philippines by the early Middle Pleistocene epoch, and long before the appearance of modern humans in both the local context and wider Island South East Asia region[21]. Although the identity of these archaic toolmakers remains unknown, it is likely that they dispersed over at least one sea barrier to reach Luzon Island[22]. The most likely points of origin are Borneo through Palawan to the west, or China through Taiwan to the north, this latter island was connected to mainland Asia during periods with low sea levels[23]. The Middle Pleistocene fauna from the Awidon Mesa Formation contains a wider range of vertebrates than the Pleistocene faunas from two islands to the south of the Philippines that have both yielded evidence of the occupation by premodern humans, Sulawesi[9] and Flores[26] (Extended Data Fig. 9). Overseas dispersal throughout Wallacea of land mammals, including hominins, could have been primarily, although not exclusively, in a north to south direction, following the major surface current flow patterns.

Beyond the chronological gap that is yet to be filled, a question clearly linked to our discovery is the origin of the Callao Cave hominin that has been dated to 66.7 ± 1 ka. This diminutive Callao hominin may represent a direct descendent from a Pleistocene migration stock related to these early Kalinga toolmakers—similar to what happened on Flores Island—or may be derived from a more recent migration wave of anatomically modern humans[6,21,24,25].

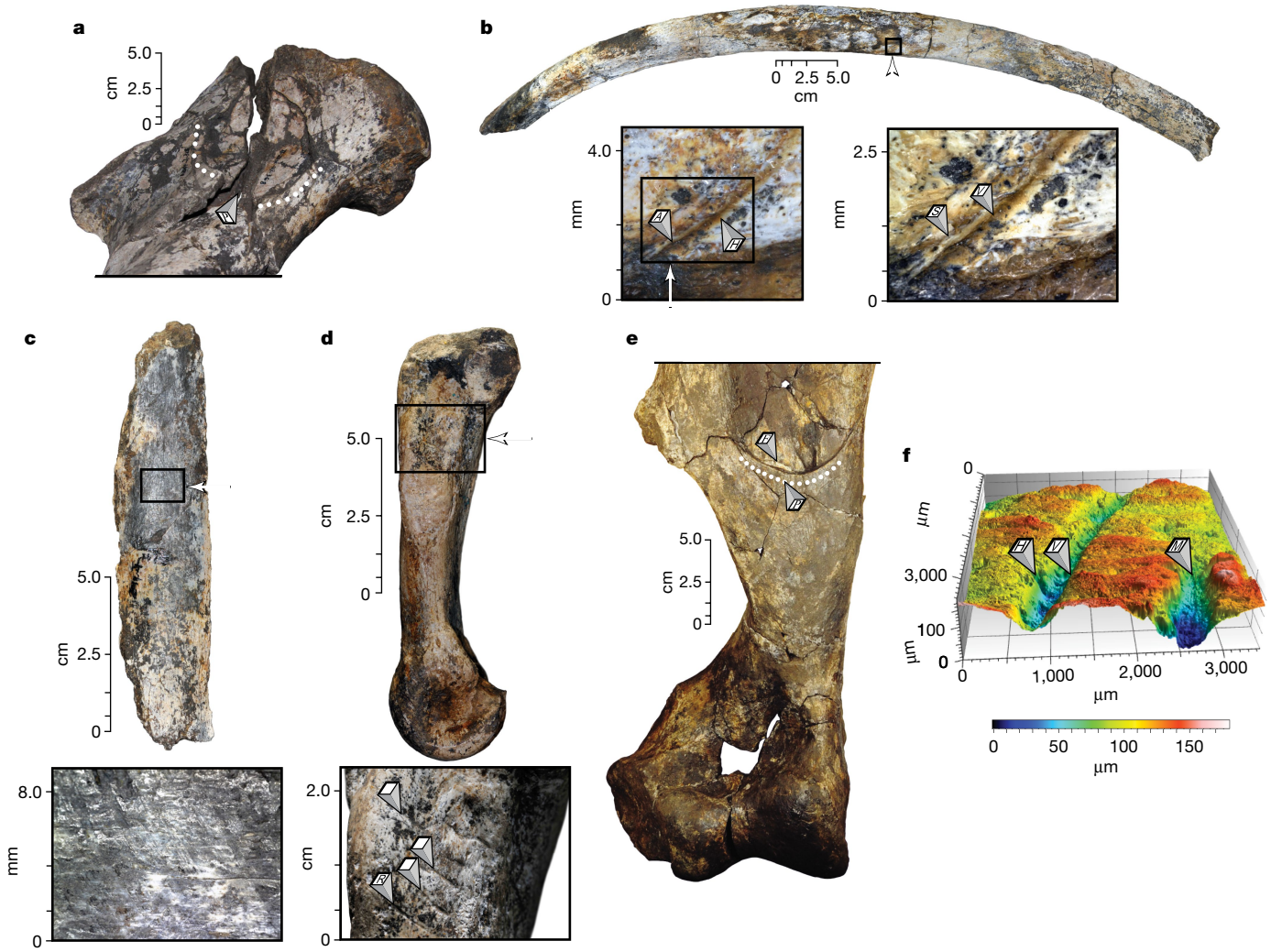

Fig. 3 | Different types of marks at the surface of the bones. a, Left humerus (II-2014-J1-368) found broken into five fragments in the excavation with an anthropogenic conchoidal percussion mark (P) on its anterior surface most likely produced to get access to the marrow. **b**, The sub-complete rib (II-2014-J1-475) has a diagnostic anthropogenic cutmark with a V-shaped cross-section (V), hertzian cones (H), asymmetrical profile (A) and shoulder effect (S) on its lateral surface resulting from defleshing. Black stains are also present inside the cutmark, which resemble the ones observed on the surface of the rib and are the result of taphonomic processes that occurred after this cutmark was made (see page 156 of Fernández-Jalvo and Andrews[17]). **c**, Rib fragment (II-2014-J1-403) with a shiny surface on its lateral face resulting from multiple multidirectional striations, which are presumably caused by trampling. **d**, Right metacarpal IV (II-2014-J1-282) with parallel and rectilinear anthropogenic cut marks (R) on its medial surface presumably generated during disarticulation. **e**, Right humerus (II-2014-J1-289) with an anthropogenic conchoidal percussion mark (P) similar in size and shape to the percussion mark on the left humerus, but located on its posterior surface and more distally and associated with a small adhered bone flake (F) (see page 298 of Fernández-Jalvo and Andrews[17]). **f**, Three-dimensional surface topography of another rib (II-2014-J1-466) showing a linear mark (on the left) with V-shaped cross-section (V) of anthropogenic origin, as well as hertzian cones (H) and a linear mark (on the right) with a base as broad as the heights of the walls of the grove, commonly attributed to trampling but also with assymetrical walls and possible microstriations in the bottom (M) of the groove, commonly attributed to anthropogenic marks.

Despite the current evidence, it still seems too farfetched to suggest that *H. erectus*, or another unknown Pleistocene ancestral candidate for the Kalinga toolmakers (for example, Denisovans[27]), were able to construct some sort of simple watercraft and deliberately cross sea barriers to reach these islands[28]. However, considering evidence of overseas dispersal during the Middle Pleistocene stage is increasing in number[29,30], such a hypothesis cannot currently be rejected.

Data availability

The datasets generated and/or analysed during the current study are available from the corresponding authors upon reasonable request.

Online content

Any Methods, including any statements of data availability and Nature Research reporting summaries, along with any additional references and Source Data files, are available in the online version of the paper at https://doi.org/10.1038/s41586-018-0072-8.

Received: 10 May 2017; Accepted: 14 March 2018;
Published online: 02 May 2018

1. Van Heekeren, H. R. Early man and fossil vertebrates on the island of Celebes. *Nature* **163**, 492 (1949).
2. Maringer, J. & Verhoeven, T. Die steinartefakte aus der *Stegodon*-fossilschicht von Mengeruda auf Flores, Indonesien. *Anthropos.* **65**, 229–247 (1970).
3. von Koenigswald, G. H. R. Preliminary report on a newly-discovered Stone Age culture from northern Luzon, Philippine Islands. *Asian Perspect.* **2**, 69–70 (1958).
4. Fox, R. B. in *Paleolithic in South and East Asia* 59–85 (Mouton Publishers, The Hague, 1978).
5. Heaney, L. R. Zoogeographical evidence for Middle and Late Pleistocene land bridges to the Philippines islands. *Mod. Quat. Res. SE Asia* **9**, 127–143 (1985).

6. Mijares, A. S. et al. New evidence for a 67,000-year-old human presence at Callao Cave, Luzon, Philippines. *J. Hum. Evol.* **59**, 123–132 (2010).
7. Ingicco, T. et al. A new species of *Celebochoerus* (Suidae, Mammalia) from the Philippines and the paleobiogeography of the genus *Celebochoerus* Hooijer, 1948. *Geobios* **49**, 285–291 (2016).
8. Brumm, A. et al. Hominins on Flores, Indonesia, by one million years ago. *Nature* **464**, 748–752 (2010).
9. van den Bergh, G. D. et al. *Homo floresiensis*-like fossils from the early Middle Pleistocene of Flores. *Nature* **534**, 245–248 (2016).
10. van den Bergh, G. D. et al. Earliest hominin occupation of Sulawesi, Indonesia. *Nature* **529**, 208–211 (2016).
11. Dizon, E. Z. & Pawlik, A. F. The lower Palaeolithic record in the Philippines. *Quat. Int.* **223–224**, 444–450 (2010).
12. Mathisen, M. & Vondra, C. The fluvial and pyroclastic deposits of the Cagayan Basin, northern Luzon, Philippines—an example of non-marine volcaniclastic sedimentation in an interarc basin. *Sedimentology* **30**, 369–392 (1983).
13. Mathisen, M. E. *Plio-Pleistocene geology of the Central Cagayan Valley, Northern Luzon, Philippines*. PhD thesis, Iowa State Univ. (1981).
14. Pawlik, A. F. The Paleolithic site of Arubo 1 in Central Luzon, Philippines. *Bull. Indo-Pacific Prehistory Assoc.* **24**, 1–10 (2004).
15. Yravedra, J. et al. Cut marks on the Middle Pleistocene elephant carcass of Áridos 2 (Madrid, Spain). *J. Archaeol. Sci.* **37**, 2469–2476 (2010).
16. Mosquera, M. et al. Barranc de la Boella (Catalonia, Spain): an Acheulean elephant butchering site from the European late Early Pleistocene. *J. Quaternary Sci.* **30**, 651–666 (2015).
17. Fernandez-Jalvo, Y. & Andrews, P. *Atlas of Taphonomic Identifications* (Springer, Dordrecht, 2016).
18. Voinchet, P. et al. ESR dating of quartz extracted from Quaternary sediments: Application to fluvial terraces system of Northern France. *Quaternaire* **15**, 135–141 (2004).
19. Lee, M.-Y., Chen, C.-H., Wei, K.-Y., Iizuka, Y. & Carey, S. First Toba supereruption revival. *Geology* **32**, 61–64 (2004).
20. Valet, J.-P. et al. Geomagnetic, cosmogenic and climatic changes across the last geomagnetic reversal from equatorial Indian Ocean sediments. *Earth Planet. Sci. Lett.* **397**, 67–79 (2014).
21. Liu, W. et al. The earliest unequivocally modern humans in southern China. *Nature* **526**, 696–699 (2015).
22. Wang, P., Li, Q. (eds). *The South China Sea: Paleoceanography and Sedimentology* Vol.13, 25–73 (Springer, Dordrecht, 2009).
23. Voris, H. K. Maps of Pleistocene sea levels in Southeast Asia: shorelines, river systems and time durations. *J. Biogeogr.* **27**, 1153–1167 (2000).
24. Détroit, F., Corny, J., Dizon, E. Z. & Mijares, A. S. "Small size" in the Philippine human fossil record: is it meaningful for a better understanding of the evolutionary history of the negritos? *Hum. Biol.* **85**, 45–66 (2013).
25. Sutikna, T. et al. Revised stratigraphy and chronology for *Homo floresiensis* at Liang Bua in Indonesia. *Nature* **532**, 366–369 (2016).
26. Brumm, A. et al. Age and context of the oldest known hominin fossils from Flores. *Nature* **534**, 249–253 (2016).
27. Cooper, A. & Stringer, C. B. Did the Denisovans cross Wallace's Line? *Science* **342**, 321–323 (2013).
28. Ruxton, G. D. & Wilkinson, D. M. Population trajectories for accidental versus planned colonisation of islands. *J. Hum. Evol.* **63**, 507–511 (2012).
29. Erlandson, J. M. & Fitzpatrick, S. M. Oceans, islands, and coasts: current perspectives on the role of the sea in human prehistory. *J. Island Coast. Archaeol.* **1**, 5–32 (2010).
30. Dennell, R. W., Louys, J., O'Regan, H. J. & Wilkinson, D. M. The origins and persistence of *Homo floresiensis* on Flores: biogeographical and ecological perspectives. *Quat. Sci. Rev.* **96**, 98–107 (2014).

Acknowledgements J. Barns and A. Labrador provided support for this research as well as G. Concepcion and M. dela Cruz Jr. The Kalinga excavation project was funded by the French Department for Foreign Affairs (Project MARCHE, to T.I.), The National Museum of The Philippines (to C.J.-o. and M.C.R.), The University of the Philippines Diliman Research Grant of the Office of Vice President for Academic Affairs (to T.I.) and the European Social Fund (Project ISOLARIO, NSRF Thalis-UOA, to G.L.). T.I. also received funding from a National Geographic Global Exploration grant (HJ-035R-17), from the French Centre National de la Recherche Scientifique (GDRi PalBiodivASE with Valéry Zeitoun), from Sorbonne Universités (Project MH@SU TAPHO), from the Société des Amis du Musée de l'Homme and from the LabEx BCDiv. G.D.v.d.B. received funding from an Australian Research Council (ARC) Future fellowship (FT100100384). J.d.V. received funding from the Quaternary and Prehistory Erasmus Mundus Program. Additional funding was provided by the Embassy of France to the Philippines and by the Rizal Municipality. M.G.C. received funding from CERCA Programme/Generalitat de Catalunya. We thank S. Hayes for her feedback on the manuscript; M.-M. Blanc-Valleron for providing access to the X-ray diffractometer; A. Ledoze, S. Puaud, V. Scao, S. Baillon, H. Guillou, J. Marteau, M. Bigerelle, R. Deltombe, D. Borshneck and F. Demory for their valuable help in the laboratory analyses.

Reviewer information *Nature* thanks M. Duval, J. Kappelman, R. Potts and the other anonymous reviewer(s) for their contribution to the peer review of this work.

Author contributions T.I., J.d.V. and A.B. conceived the study with C.J-o. and G.D.v.d.B. in collaboration with N.A., G.L., P.C.H.A. and M.L. The site stratigraphy was recorded and analysed by G.D.v.d.B. Samples for ESR/U-series dating were analysed by J.-J.B., Q.S. and C.F. Samples for ESR dating on quartz were analysed by P.V. Samples for $^{40}Ar/^{39}Ar$ dating were analysed by S.N. and A.P. D.Y. analysed samples for palaeomagnetism. P.R. analysed the tektite. The lithic material was studied by H.F. and M.G.C. Palaeobotanical remains were analysed by A.-M.S. and C.K. The faunal and taphonomical analysis was conducted by T.I., K.M., M.C.R. and N.A. T.I. and G.v.d.B. wrote the manuscript.

Competing interests The authors declare no competing interests.

Additional information

Extended data is available for this paper at https://doi.org/10.1038/s41586-018-0072-8.
Supplementary information is available for this paper at https://doi.org/10.1038/s41586-018-0072-8.
Reprints and permissions information is available at http://www.nature.com/reprints.
Correspondence and requests for materials should be addressed to T.I. or M.C.R.

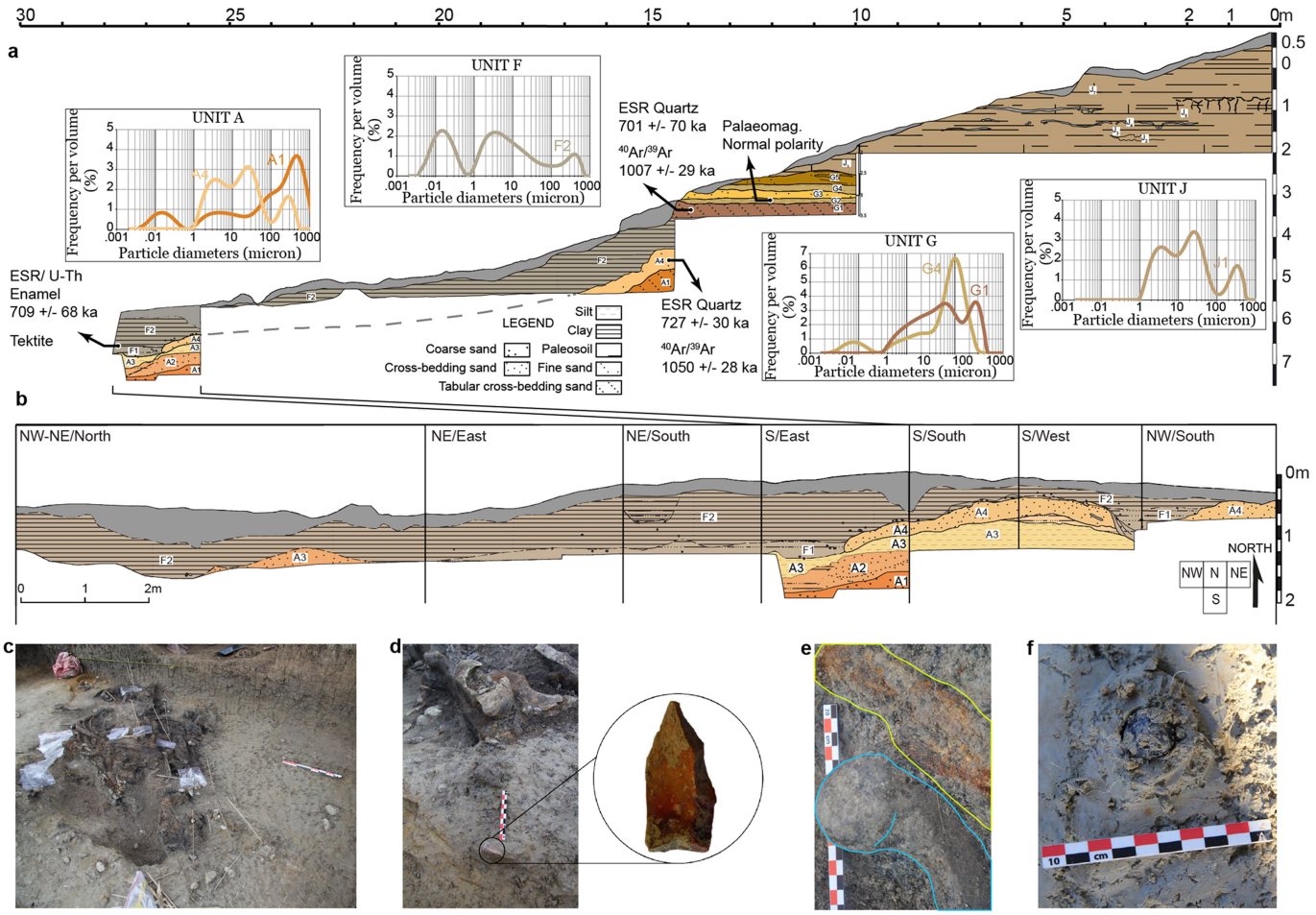

Extended Data Figure 1 | Geology and sedimentology of the Kalinga Excavation site. a, Detailed stratigraphic drawing of trench H also showing the east wall of the S quadrant of the main excavation. The sedimentary patterns are the same as in Fig. 1. Representative logarithmic grain-size diagrams are shown for samples from each sedimentary unit. **b**, Detailed stratigraphic drawing of the main excavation walls. **c**, Overview towards the northwest of the quadrants N and NW of the main excavation in 2015. The concentration of faunal remains and stone tools lying at the base of unit F is exposed, just above the eastward sloping erosional contact with unit A. **d**, Detailed view of quadrant NW showing the position of a flake lying next to the rhinoceros left femur. **e**, Detail of quadrant N showing the piece of waterlogged wood fragment (yellow outline) recovered near a rhinoceros rib extremity (blue outline). **f**, Detail of quadrant NE showing the tektite recovered in unit F along with the faunal and lithic remains.

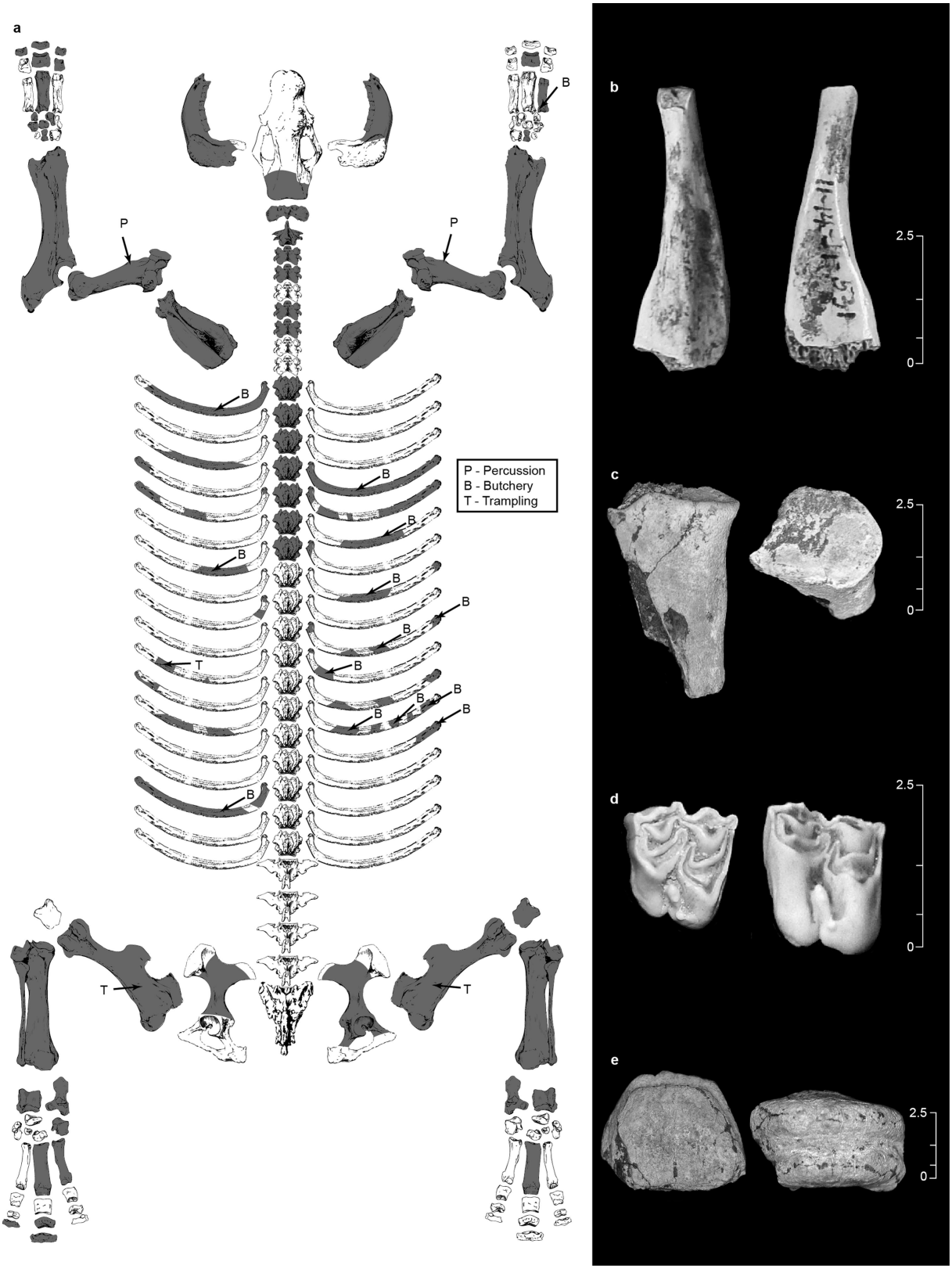

Extended Data Figure 2 | Faunal remains from Kalinga archaeological unit F. a, Drawing showing the preservation of the rhinoceros and position of the taphonomical marks. A total of 97 fragments of ribs of all sizes have been recovered and not all of them could be clearly positioned on the skeleton. We estimate that about 75% of the skeleton has been recovered. **b**, Fibula of *Varanus salvator*. **c**, Radius of a Cervidae. **d**, Molar of *Cervus* cf. *mariannus*. **e**, Molar fragment of *Stegodon* cf. *luzonensis*.

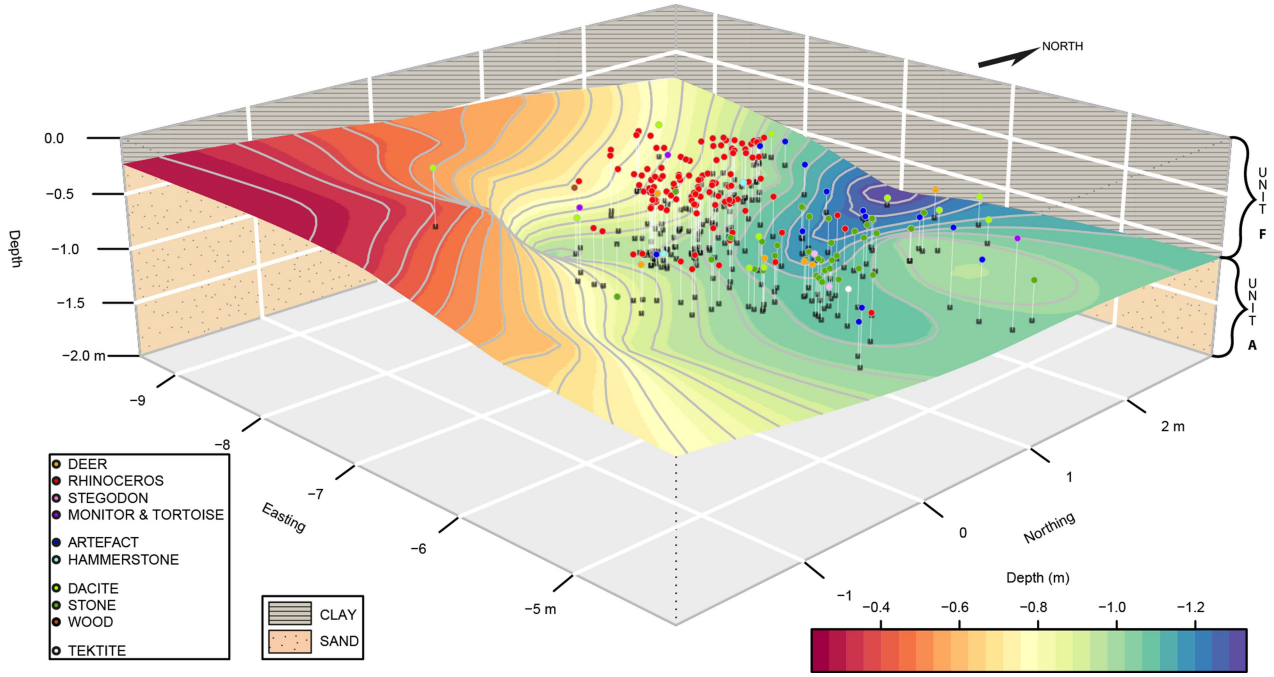

Extended Data Figure 3 | Digital elevation model of the main Kalinga excavation. The model shows the contact surface topography between unit A and unit F and the vertical projections (black squares) of the archaeological materials (coloured points) on this surface. The model was produced by interpolation through a kriging method from 37 three-dimensional coordinates recorded in the main excavation with a total station on the erosional surface that cuts down into unit A. This surface of contact corresponds to an erosional channel cutting down into the sandy unit A. All the material has been recovered lying across the base of the clay-rich unit F along this channel, between 0.7 m and 1.3 m deep.

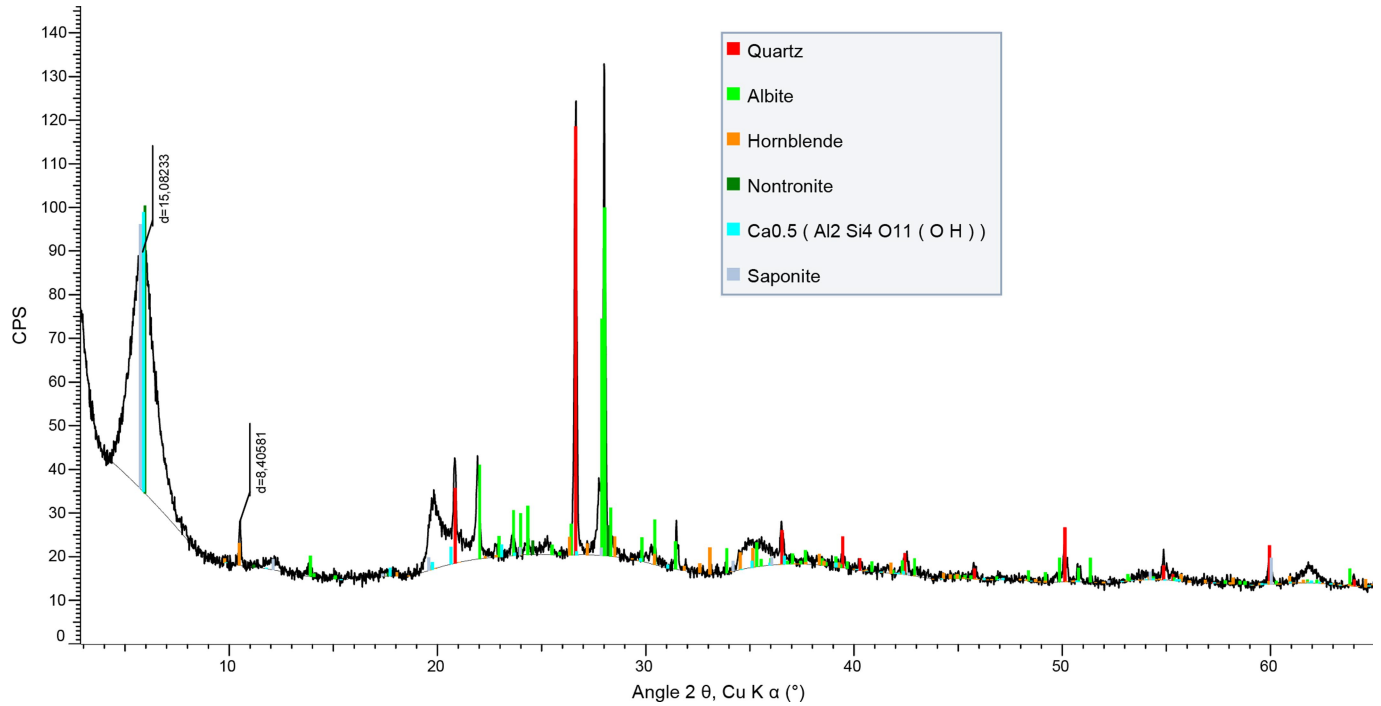

Extended Data Figure 4 | X-ray diffraction pattern of powdered unit F clays. Quartz corresponds to the bipyramidal quartz crystals, some of which are visible to the naked eye. Bipyramidal quartz, albite, hornblende, nontronite and saponite all have a volcanic origin. Albite is a plagioclase feldspar frequent in pegmatites. Hornblende is a common silicate mineral in igneous and metamorphic rocks. Nontronite is an iron-rich smectite type of clay, which can be produced by hydrothermal alteration. Similarly, the smectite mineral saponite results from alteration of volcanic glass. The mineral composition of unit F supports the interpretation as a mudflow set in a volcanic environment. CPS, counts per second; Cu K-α corresponds to the wavelength.

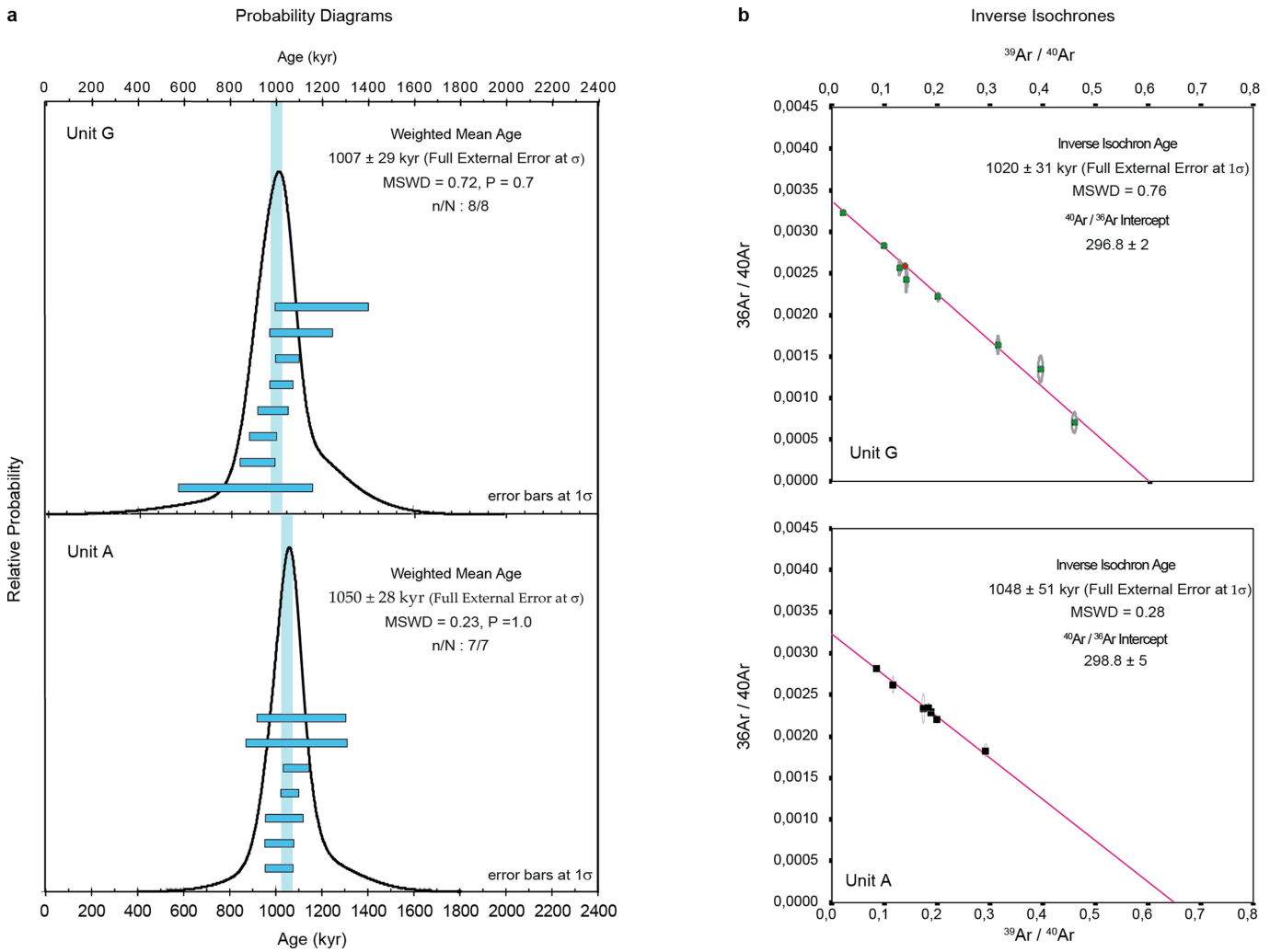

Extended Data Figure 5 | $^{40}Ar/^{39}Ar$ fusion ages of single potassium plagioclase crystals for samples from unit A and unit G. a, **b**, Probability diagrams (**a**) are correlated to the related inverse isochrones (**b**). Individual ages in **a** are $\pm 1\sigma$.

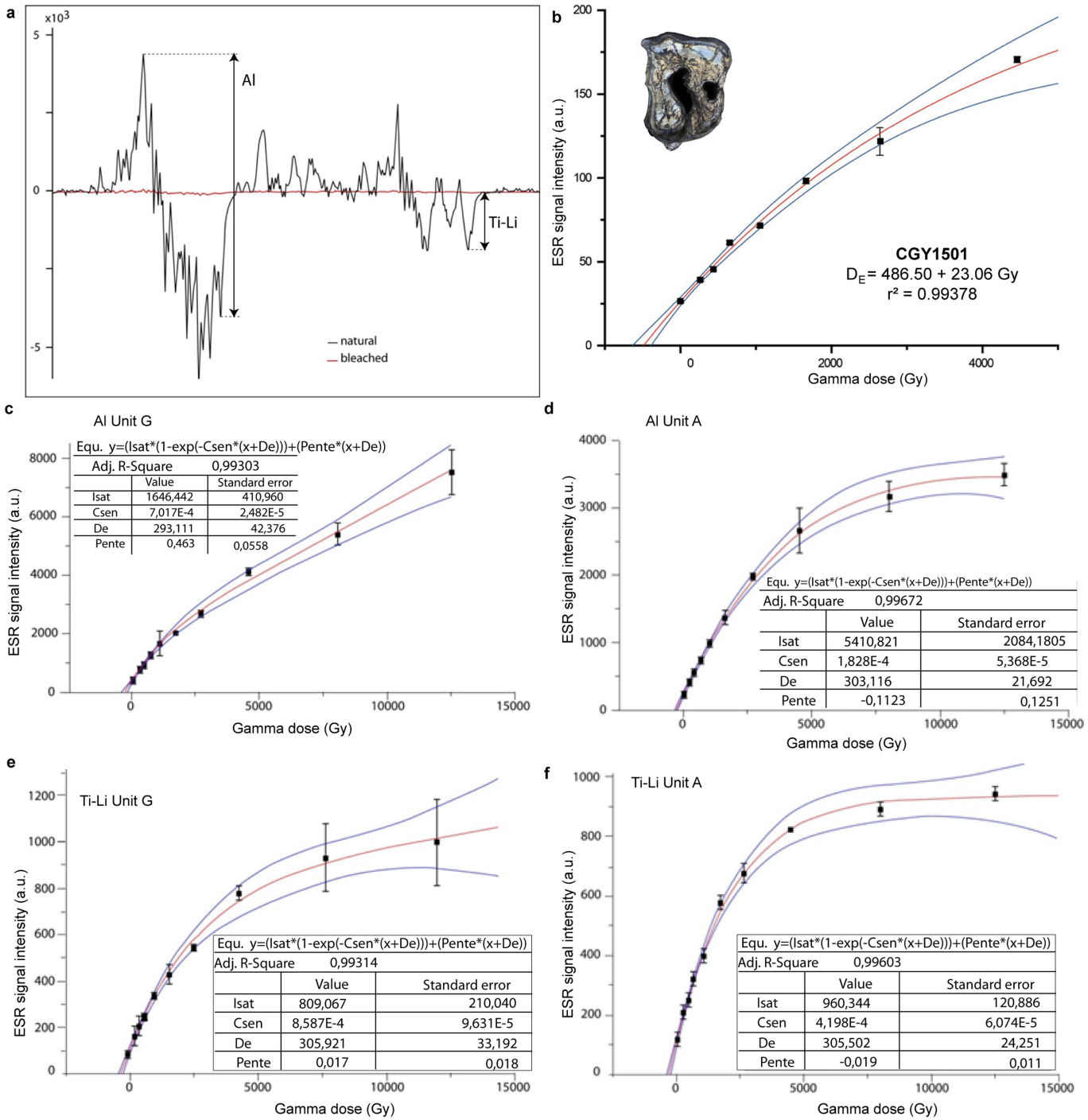

Extended Data Figure 6 | Measurements of dose rates and calculation of equivalent dose to compute the ESR ages from quartz crystals and tooth enamel. a, Al and Ti centre ESR spectra of natural and bleached aliquots for unit A quartz showing that the Al signal is not completely reset, although it is not measurable because it is extremely weak and concealed by noise. **b**, ESR dose–response curve obtained for the rhinoceros tooth (archaeological number: II-2014-J1-095; sample code: CGY1501). The equivalent dose (D_e) was extrapolated using a single saturating exponential function (Origin Microcal software) following the recommendations of Duval and Grün[31] ($D_e < 500$ Gy, therefore $D_{max} < 5{,}000$ Gy for this sample). **c**–**f**, ESR dose–response curves, for the aluminium (Al) and titanium–lithium (Ti-Li) centres of layers G1 and A4. **b**–**f**, The vertical bars indicate the standard deviation around the mean for each measurement. The red curve is the dose–response curve. The blue curves indicate the 95% confidence interval of the dose–response curve.

31. Duval, M. & Grün, R. Are published ESR dose assessments on fossil tooth enamel reliable? *Quat. Geochronol.* **31**, 19–27 (2016).

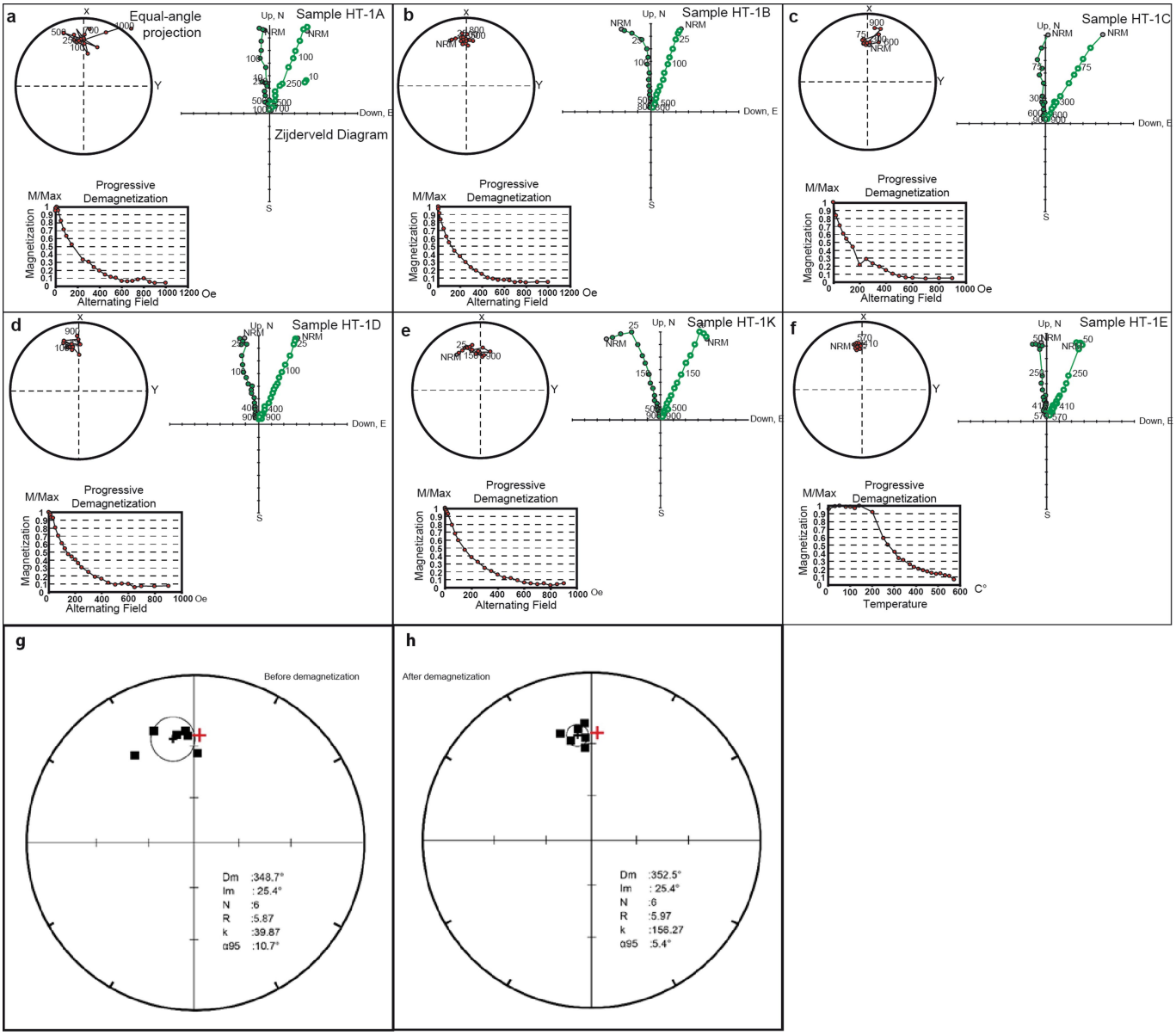

Extended Data Figure 7 | Progressive demagnetization curves, equal area projection stereoplots and Zijderveld diagrams for the six analysed specimens from Layer G_2. a–f, Each panel shows the progressive demagnetization curves (bottom left), equal area projection stereoplots (top left) and Zijderveld diagrams (right). Open circles in the Zijderveld diagrams represent the inclination whereas closed circles represent declination. Open and closed circles in the equal area projection (stereoplot) represent the upper and lower hemisphere, respectively. **a–e**, Specimens were treated by alternating field demagnetization. **f**, Specimen HT-1E was treated by thermal demagnetization. **g**, **h**, Equal area projections of the mean chemical remanent magnetization (ChRM) directions of all analysed specimens before (**g**) and after (**h**) demagnetization. Solid squares represent the upper hemisphere. The black cross indicates the mean ChRM direction of the six specimens combined, surrounded by the α95 circle. The red cross represents the present-day magnetic direction.

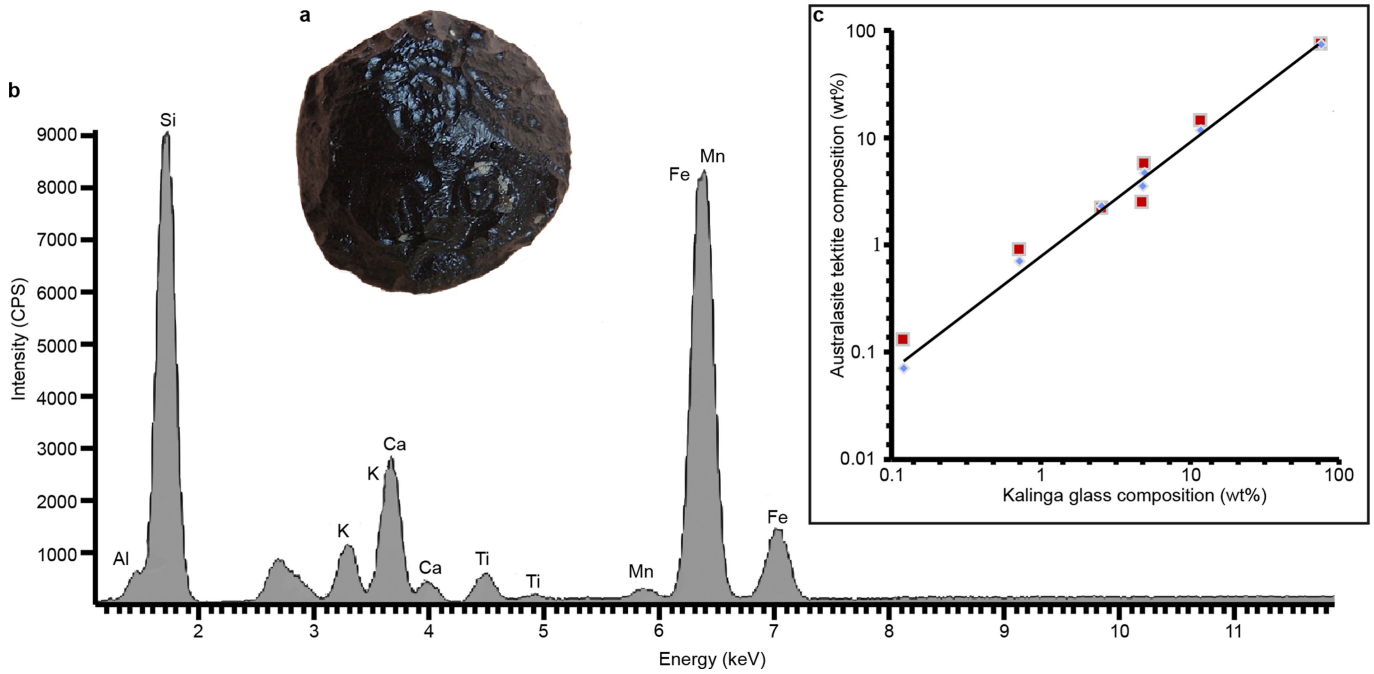

Extended Data Figure 8 | Analysis of the Kalinga tektite recovered from the archaeological layer unit F. a, Picture of the tektite. **b**, Micro-X-ray fluorescence (μXRF) spectra (un-indexed peaks correspond to the Rh source) showing its composition. **c**, Comparison of the Kalinga tektite glass composition through μXRF to an australasite tektite from China measured in the same conditions (red squares) and an average australasite composition (blue diamonds)[32].

32. Koeberl, C. The geochemistry of tektites: an overview. *Tectonophysics* **171**, 405–422 (1990).

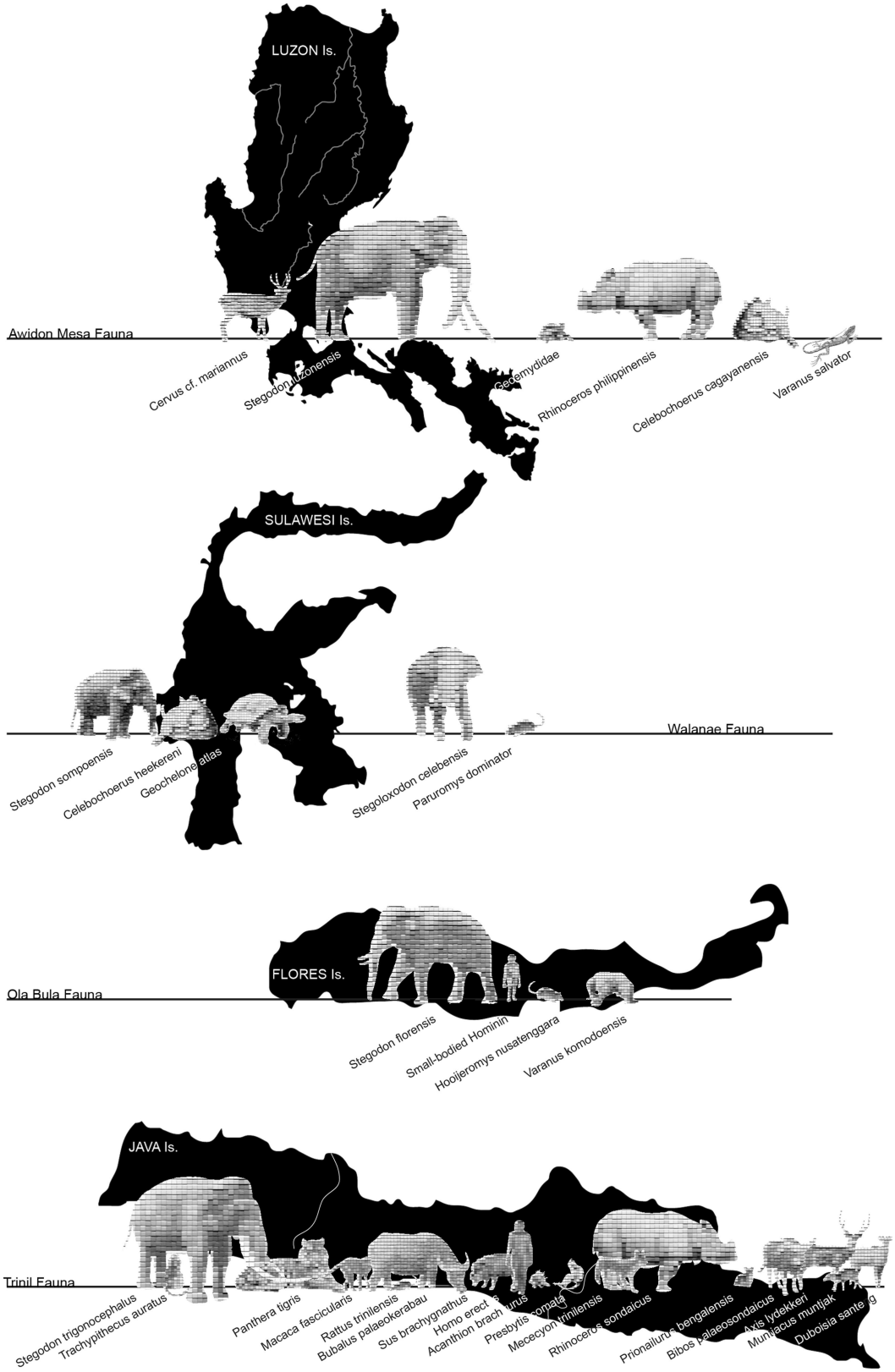

Extended Data Figure 9 | Fauna diversity of the Kalinga site compared to contemporaneous faunas from other islands in the region. Contemporaneous to those faunas are 'classic' *H. erectus* faunas on Java Island[33], the Mata Menge Fauna of Flores Island, which includes the putative ancestor of *H. floresiensis*[34], and the Walanae Fauna on the southwestern branch of Sulawesi[35,36].

33. De Vos, J., Sartono, S., Hardja-Sasmita, S. & Sondar, P.-Y. The fauna from Trinil, type locality of *Homo erectus* a reinterpretation. *Geologie Mijnbouw* **61**, 207–211 (1982).
34. van den Bergh, G. D. et al. *Homo floresiensis*-like fossils from the early Middle Pleistocene of Flores. *Nature* **534**, 245–248 (2016).
35. van den Bergh, G. D., de Vos, J. & Sondaar, P. Y. The Late Quaternary palaeogeography of mammal evolution in the Indonesian Archipelago. *Palaeogeogr. Palaeoclimatol. Palaeoecol.* **171**, 385–408 (2001).
36. Downing, K. F., Musser, G. G. & Park, L. E. in *Advances in Vertebrate Paleontology and Geochronology* Vol. 14 (eds Tomida, Y. et al.) 105–121 (National Science Museum Monographs, Tokyo, 1998).

Extended Data Table 1 | ESR/U-series results for the rhinoceros tooth

a

Sample	Tissue	U (ppm)	$^{234}U/^{238}U$	$^{230}Th/^{232}Th$	$^{230}Th/^{234}U$	$^{2220}Rn/^{230}Th$	Apparent U-series ages[1] (ka±2σ)
IPH-2015-09 CGY1501 (R-2014-J1-095)	dentine	52.3336 ± 0.1692	1.3701 ± 0.0062	141.40	0.8950 ± 0.0051	1.000	**220.70** ± 3.28
	enamel	0.2356 ± 0.0001	1.2564 ± 0.0009	48.96	0.8147 ± 0.0014	0.976	**164.86** ± 0.96

b

Sample	Tissue	Palaeodose D_E (Gy)	U uptake parameter p	$D_{a\,\alpha}$ Internal [1] (μGy/a)	$D_{a\,\beta}$ [2] dent+sed (μGy/a)	$D_{a\,\beta1}$ dentine (μGy/a)	$D_{a\,\beta2}$ sediment (μGy/a)	D_{a1} γ (μGy/a)	D_{a2} cosmic (μGy/a)	D_a total (μGy/a)	ESR/U-series ages US [4] (ka±1σ)
IPH-2015-09 CGY1501 (R-2014-J1-095)	dentine	486.50 ± 23.06	-0.1636 ± 0.0447	47 ± 8	258 ± 35	208 ± 35	50 ± 4	242 ± 12	145 ± 10	692 ± 38	**709 ± 58**
	enamel		0.3834 ± 0.0765								

a, U-series data for the tooth CGY1501. **b**, ESR/U-series data and age. Eventual radium and radon losses from the dental tissues were estimated from cross-checked γ and α data[37]. Dose conversion factors were used according to previously published data[38]. Water contents of 0 ± 0%, 7 ± 5% and 10 ± 5% were used for enamel (fixed), dentine (fixed) and sediments (difference in mass between the natural sample and the same sample dried for a week in an oven at 50 °C), respectively.

[1]A *k*-value of 0.13 ± 0.02 was used following a previously published study[38].

[2]The enamel thickness removed during the preparation process was taken into account in the β contribution calculation[39]. The following values were used for the age calculation: 1,505 ± 376 μm, 351 ± 88 μm and 45 ± 12 μm for the initial thickness, thickness after preparation on the dentine side and on the sediment side, respectively.

[3]The cosmic dose was estimated based on the depth using Prescott and Hutton's formulae[40]. Because we have at present no means to know precisely when the erosion took place and since when the archaeological material became buried under less than 7 m of sediment, a depth of 2.75 m was used for the cosmic dose rate estimation as an intermediate value between the 7 m of sediments that once covered the archaeological layer and the present 70 cm to 1.20 m depth at which the archaeological material was recovered, and as an average between the once full thickness of the archaeological layer and the present thickness from which the archaeological material was recovered. A cosmic dose estimated from a depth of 7 m would result in a 10% older age for unit F and a cosmic dose estimated from a depth of 1 m would result in a 7% younger age for unit F.

[4]Uncertainties on the ESR/U-series ages were calculated using Monte Carlo approach[41].

37. Bahain, J.-J., Yokoyama, Y., Falguères, C. & Sarcia, M. N. ESR dating of tooth enamel: a comparison with K–Ar dating. *Quat. Sci. Rev.* **11**, 245–250 (1992).
38. Grün, R. & Katzenberger-Apel, O. An alpha irradiator for ESR dating. *Anc. TL* **12**, 35–38 (1994).
39. Brennan, B. J., Rink, W. J., McGuirl, E. L., Schwarcz, H. P. & Prestwich, W. V. Beta doses in tooth enamel by "one-group" theory and the ROSY ESR dating software. *Radiat. Meas.* **27**, 307–314 (1997).
40. Prescott, J. R. & Hutton, J. T. Cosmic ray contributions to dose rates for luminescence and ESR dating: large depths and long-term time. *Radiat. Meas.* **23**, 497–500 (1994).
41. Shao, Q., Bahain, J.-J., Dolo, J.-M., Falguères, C. Monte Carlo approach to calculate US-ESR ages and their uncertainties. *Quat. Geochronol.* **22**, 99–106 (2014).

nature research

Corresponding author(s): Thomas INGICCO

☐ Initial submission ☒ Revised version ☐ Final submission

Life Sciences Reporting Summary

Nature Research wishes to improve the reproducibility of the work that we publish. This form is intended for publication with all accepted life science papers and provides structure for consistency and transparency in reporting. Every life science submission will use this form; some list items might not apply to an individual manuscript, but all fields must be completed for clarity.

For further information on the points included in this form, see Reporting Life Sciences Research. For further information on Nature Research policies, including our data availability policy, see Authors & Referees and the Editorial Policy Checklist.

Experimental design

1. Sample size

Describe how sample size was determined.

ESR-U/Th, Methods p.3 L79. ESR, Methods p.4 L101. Ar/Ar. Methods p.6 L157. Paleomag, Methods p.8 L193

2. Data exclusions

Describe any data exclusions.

Not Applicable

3. Replication

Describe whether the experimental findings were reliably reproduced.

Not Applicable

4. Randomization

Describe how samples/organisms/participants were allocated into experimental groups.

Not Applicable

5. Blinding

Describe whether the investigators were blinded to group allocation during data collection and/or analysis.

Not Applicable

Note: all studies involving animals and/or human research participants must disclose whether blinding and randomization were used.

6. Statistical parameters

For all figures and tables that use statistical methods, confirm that the following items are present in relevant figure legends (or in the Methods section if additional space is needed).

n/a	Confirmed	
☐	☒	The exact sample size (*n*) for each experimental group/condition, given as a discrete number and unit of measurement (animals, litters, cultures, etc.)
☐	☒	A description of how samples were collected, noting whether measurements were taken from distinct samples or whether the same sample was measured repeatedly
☒	☐	A statement indicating how many times each experiment was replicated
☐	☒	The statistical test(s) used and whether they are one- or two-sided (note: only common tests should be described solely by name; more complex techniques should be described in the Methods section)
☒	☐	A description of any assumptions or corrections, such as an adjustment for multiple comparisons
☐	☒	The test results (e.g. *P* values) given as exact values whenever possible and with confidence intervals noted
☐	☒	A clear description of statistics including central tendency (e.g. median, mean) and variation (e.g. standard deviation, interquartile range)
☐	☒	Clearly defined error bars

See the web collection on statistics for biologists for further resources and guidance.

Software

Policy information about availability of computer code

7. Software

Describe the software used to analyze the data in this study.	ESR dose rates were calculated using Microcal OriginPro 8 software. Ar/Ar weighted average ages were calculated using IsoPlot Mean ChRMs palaeomagnetism directions were determined using Puffin Plot Software

For manuscripts utilizing custom algorithms or software that are central to the paper but not yet described in the published literature, software must be made available to editors and reviewers upon request. We strongly encourage code deposition in a community repository (e.g. GitHub). *Nature Methods* guidance for providing algorithms and software for publication provides further information on this topic.

Materials and reagents

Policy information about availability of materials

8. Materials availability

Indicate whether there are restrictions on availability of unique materials or if these materials are only available for distribution by a for-profit company.	Not Applicable

9. Antibodies

Describe the antibodies used and how they were validated for use in the system under study (i.e. assay and species).	Not Applicable

10. Eukaryotic cell lines

a. State the source of each eukaryotic cell line used.	Not Applicable
b. Describe the method of cell line authentication used.	Not Applicable
c. Report whether the cell lines were tested for mycoplasma contamination.	Not Applicable
d. If any of the cell lines used are listed in the database of commonly misidentified cell lines maintained by ICLAC, provide a scientific rationale for their use.	Not Applicable

Animals and human research participants

Policy information about studies involving animals; when reporting animal research, follow the ARRIVE guidelines

11. Description of research animals

Provide details on animals and/or animal-derived materials used in the study.	Not Applicable

Policy information about studies involving human research participants

12. Description of human research participants

Describe the covariate-relevant population characteristics of the human research participants.	Not Applicable